Gersch-Rodriguez-Smith computation of deep inelastic electron scattering on ^{4}He

M. Viviani and A. Kievsky
INFN, Sezione Pisa, and Physics Department, University of Pisa, I-56100 Pisa, Italy

A. S. Rinat
Department of Particle Physics, Weizmann Institute of Science, Rehovot 76100, Israel

(Received 16 November 2001; revised manuscript received 22 November 2002; published 12 March 2003)

We compute cross sections for inclusive scattering of high-energy electrons on ^{4}He, based on the two lowest orders of the Gersch-Rodriguez-Smith series. The required one- and two-particle density matrices are obtained from nonrelativistic ^{4}He wave functions using realistic models for the nucleon-nucleon and three-nucleon interaction. The computed results for $E=3.6$ GeV agree well with the NE3 SLAC-Virginia data.

DOI: 10.1103/PhysRevC.67.034003 PACS number(s): 25.30.Fj, 13.60.Hb

I. INTRODUCTION

It is appealing to describe the total nuclear structure function (SF) in terms of the SF of a nucleon, linking the two through a representative property of the medium. It is broadly accepted that the above link is represented by the SF of a nucleus composed of point-nucleons, the internal structure of which resides in the SF of a nucleon. Such a program is usually performed within one of the following two approaches. In the first, one perturbatively expands the SF of the point-nucleon system in the residual interaction between a nucleon struck by the virtual photon and the remaining spectator nucleus, thus generating the impulse series (IS) for the SF. In the widely used lowest order impulse approximation, this residual interaction is first neglected. One then either computes higher order final state interaction (FSI) terms (see, for instance, Refs. [1,2]), or models them [3–6].

An alternative approach is based on a relativistic generalization of the Gersch-Rodriguez-Smith (GRS) expansion of the SF of a nucleus of point particles in inverse powers of the three-momentum transfer $|\boldsymbol{q}|$ [7–9]. Both theories have been applied to cross sections for inclusive scattering of high-energy leptons from various nuclear targets [3–6,10,11].

When applied to high-energy inclusive scattering, one usually limits a GRS calculation to the two lowest order terms. Their determination requires knowledge of one- and two-particle density matrices, which are not diagonal in the coordinate of the struck nucleon $'1'$, and of the spectral function. The nondiagonal one-body density matrix is related to the single-nucleon momentum distribution $n(p)$ and is usually extracted from alternative experimental sources, or is computed from theoretical models. There generally is no direct information on the half-diagonal, two-particle density matrices for finite systems and one relies on parametrizations [7,12]. In those, nuclear recoil is usually neglected, thereby limiting applications to targets with $A \gtrsim 12$.

In the following, we exploit accurately computed nonrelativistic (NR) wave functions for light nuclei, using a number of modern realistic nucleon-nucleon (NN) and three-nucleon ($3N$) interactions. Those wave functions are Galilean invariant and enable a realistic GRS calculation of inclusive scattering on those nuclei. As a first application, we choose ^{4}He and for that target we shall report below a comparison with the $E=3.6$ GeV SLAC-Virginia data [13].

The other ingredient, namely, the ^{4}He spectral function $\mathcal{P}(p,\mathcal{E})$, is rather difficult to compute and only a few direct calculations are reported [14,15]. Below we shall adopt the reasonable alternative that has been developed by Ciofi degli Atti and Simula [6]. The importance of using realistic spectral functions when comparing with data is well known and it has been also remarked in Ref. [16].

At this point we mention that for years the IS and GRS approaches have been considered as being distinct and even incompatible. Only recently has their equivalence been demonstrated, provided both series are expanded to the same order in the same parameter [2,8,9]. Following the derived prescription to link the two approaches, one can perform an interesting numerical comparison.

The GRS and IS theories are not the only tools which have been used to compute nuclear SF's. We mention in particular the ingenious method of Efros and co-workers, which has been applied to ^{4}He [15,17]. Regrettably, it appears not feasible to extend that method to high energies.

The main goals of this paper are the following. (i) The first study of the leading two terms in the GRS series applied to ^{4}He and a comparison of the results with the good quality ^{4}He SLAC-Virginia data. (ii) To establish for the case at hand the relative importance of FSI versus the lowest order term, in particular in the low-energy loss region. (iii) To present a first comparison between the GRS and IS expansions, cut at the same order in $1/|\boldsymbol{q}|$ for a real system, in contrast to what has been done in the past for models (see, for instance, Ref. [19]).

We also present in the paper predictions for the foreseen $E=6$ GeV experiment at JLab on ^{4}He [18]. Since the accuracy of the underlying theory [embodied in the convolution integral given in Eq. (2.2)] grows with the squared momentum transfer Q^2, a comparison of theoretical results and data in the deep inelastic region may enable the extraction of the neutron structure function at those Q^2.

The present paper is organized as follows. In Sec. II, we recall the GRS approach, emphasizing the two main ingredients of our calculations, namely, the SF of a target composed of point particles and the SF of the free nucleons. We also discuss there the computation of the above density matrices. In Sec. III, we compare our computed results for cross sec-

tions with the Virginia-SLAC data [13]. In the last section, we present our conclusions.

II. TOTAL NUCLEAR STRUCTURE FUNCTIONS

The cross section per nucleon for inclusive scattering of high-energy electrons from a nucleus with A nucleons reads

$$\frac{d^2\sigma_{eA}(E;\theta,\nu)/A}{d\Omega\, d\nu} = \frac{2}{M}\sigma_M(E;\theta,\nu)\left[\frac{xM^2}{Q^2}F_2^A(x,Q^2) + \tan^2(\theta/2)F_1^A(x,Q^2)\right], \tag{2.1}$$

where M is the nucleon mass, σ_M is the Mott cross section, E is the beam energy, θ is the laboratory scattering angle, and ν is the energy loss imparted onto the target. The above nuclear structure functions per nucleon $F_k^A(x,Q^2)$ contain the essence of unpolarized electron scattering from randomly oriented targets. Those SF's depend on the squared four momentum transfer $-q^2=Q^2=|\boldsymbol{q}|^2-\nu^2$ and on the Bjorken variable $x=Q^2/2M\nu$ with range $0\leqslant x\leqslant A$. For given beam energy E,(θ,ν) and (x,Q^2) are sets of alternative kinematic variables.

Total nuclear structure functions per nucleon may, in a semiheuristic fashion, be expressed as follows [20–22]:

$$F_k^A(x,Q^2) = \int_x^A \frac{dz}{z^{2-k}} f^{PN,A}(z,Q^2) \times \sum_{l=1}^{2} C_{kl}\left(\frac{Q^2}{x^2},z\right) F_l^{\langle N\rangle}\left(\frac{x}{z},Q^2\right). \tag{2.2}$$

In the equation above, $f^{PN,A}$ is the SF of a nucleus composed of point particles, and $F_k^{\langle N\rangle}$ is the averaged nucleon SF, weighted by the number of protons and neutrons in the nucleus $A(Z,N)$

$$F_k^{\langle N\rangle}(x,Q^2) = \frac{Z}{A}F_k^p(x,Q^2) + \frac{N}{A}F_k^n(x,Q^2), \quad k=1,2. \tag{2.3}$$

We consider F^p (F^n) to be the free proton (neutron) SF. One may then interpret the nuclear SF per nucleon given by Eq. (2.2) as those nucleon SF's modified by the medium, brought about by $f^{PN,A}$.

The coefficient functions C_{kl} account for the mixing of the nucleon structure functions in the expression (2.2) [23]. We retain in this paper only the dominant coefficient

$$C_{22}\left(\frac{Q^2}{x^2},z\right) \approx [1-\rho+\rho/z]^2 - \frac{1}{2}\rho(1-\rho)(1-1/z)^2,$$
$$\rho = [1+Q^2/4M^2x^2]^{-1}. \tag{2.4}$$

Equation (2.4) is a better approximation for C_{22} than previously used [22].

Equation (2.2) is valid for $x\gtrsim 0.15$–0.20, below which pionic and antiscreening effects become of importance [24] and above some critical Q_c^2, which presumably can be estimated using QCD. A previous comparison of computed results and data for medium-A targets produced an empirical estimate $Q^2\gtrsim Q_c^2\approx 2.0$–$2.5$ GeV^2 [11].

Each of the SF $F_k^{p,n}$ in Eq. (2.2) has both nucleon-elastic (NE) and nucleon-inelastic (NI) parts, thus $F_k^N = F_k^{N,\mathrm{NE}} + F_k^{N,\mathrm{NI}}$, with $N=p,n$. The total nuclear structure functions, Eq. (2.2), and the total cross section per nucleon may therefore be expressed as a sum over contributions coming from the NE and NI parts of nucleon SF. In particular, the NE part $F_k^{N,\mathrm{NE}}$ is the well-known combination of static electromagnetic form factors and contributes primarily around the region of the quasi-elastic peak (QEP), $x\approx 1$. For the inelastic parts $F_k^{n,\mathrm{NI}}$ we have taken

$$F_k^{n,\mathrm{NI}}(x,Q^2) \approx F_k^{d,\mathrm{NI}}(x,Q^2) - F_k^{p,\mathrm{NI}}(x,Q^2), \quad k=1,2, \tag{2.5}$$

where $F_k^{d,\mathrm{NI}}(x,Q^2)$ are the deuteron SF's per nucleon. For $F_1^{p,\mathrm{NI}}(x,Q^2)$ and $F_1^{d,\mathrm{NI}}(x,Q^2)$ we employ values interpolated between the data of Ref. [25], whereas for $F_2^{p,\mathrm{NI}}(x,Q^2)$ and $F_2^{d,\mathrm{NI}}(x,Q^2)$ we use the parametrizations of Ref. [26]. Later on one would like to use more realistic neutron SF, for instance by using Eq. (2.2) in the inverse sense, namely, to extract $F_k^{n,\mathrm{NI}}$ employing high-quality data on F^A, F^p and the computed $f^{PN,A}$ (for a first attempt, see Ref. [27]).

A. The GRS series

We now focus on $f^{PN,A}$ in Eq. (2.2), the SF for a nucleus of point particles, which has to be computed. Following Ref. [10] one writes

$$f^{PN,A}(x,Q^2) = \left(\frac{\partial y_G}{\partial x}\right)_{Q^2\ \mathrm{fixed}} \phi(|\boldsymbol{q}|,y_G),$$
$$|\boldsymbol{q}| = Q\sqrt{1+(Q/2Mx)^2}, \tag{2.6}$$

where $\phi(|\boldsymbol{q}|,y)$ is the reduced response in terms of a relativistic scaling variable [8]

$$y_G = y_G^{\Delta} \approx y_G^{\infty}\left[1-\frac{1}{2A'}\frac{\nu^2}{|\boldsymbol{q}|^2}\xi + \mathcal{O}(1/A'^2)\right], \quad A'=A-1,$$
$$y_G^{\infty} = \frac{M\nu}{|\boldsymbol{q}|}\xi,$$
$$\xi = \left(1-\frac{\langle\Delta\rangle}{M}-x\right), \tag{2.7}$$

and $\langle\Delta\rangle$ some average nucleon separation energy. We shall retain the above $1/A'$ correction in the scaling variable y_G which, as Eq. (2.7) shows, is simply related to the Bjorken variable x. In the GRS approach the reduced response may, for smooth NN interactions, be expanded in a series of inverse powers of $|\boldsymbol{q}|$ [7,9]. Explicitly

$$\phi(|\boldsymbol{q}|,y_G)=\phi_0(|\boldsymbol{q}|,y_G)+\sum_{n\geqslant 1}\left(\frac{M}{|\boldsymbol{q}|}\right)^n\phi_n(y_G). \quad (2.8)$$

The lowest order term is given by

$$\phi_0(|\boldsymbol{q}|,y_G^{\Delta_0})=\int_{|y_G^{\Delta_0}|}^{\infty}\frac{dp\,p}{4\pi^2}\int_0^{E_M}d\mathcal{E}\mathcal{P}(p,\mathcal{E}) + \theta(y_G^{\Delta_0})\int_0^{y_G^{\Delta_0}}\frac{dp\,p}{4\pi^2}\int_{E_m}^{E_M}d\mathcal{E}\,\mathcal{P}(p,\mathcal{E}), \quad (2.9)$$

with $\mathcal{P}(p,\mathcal{E})$ the standard single-hole spectral function. The energy argument is $\mathcal{E}=E-\Delta_0$ with E the removal energy and Δ_0 the (p,n averaged) minimal separation energy (for ^{4}He $\Delta_0\approx 20.2$ MeV). Above, $y_G^{\Delta_0}$ is the scaling variable give in Eq. (2.7) with $\langle\Delta\rangle=\Delta_0$. The integration limits in Eq. (2.9) are

$$E_m^M(y_G,p,|\boldsymbol{q}|)=\frac{(y_G\pm p)|\boldsymbol{q}|}{\nu}. \quad (2.10)$$

In actual calculations the spectral function has been written as in Ref. [28],

$$\mathcal{P}(p,\mathcal{E})=n_0(p)\,\delta(\mathcal{E})+\mathcal{P}_1(p,\mathcal{E}), \quad (2.11)$$

where $n_0(p)$ is the partial momentum distribution due to intermediate states of one nucleon and the $A-1$ spectator system in its ground state. Contributions from continuum states of that system are summed in $\mathcal{P}_1(p,\mathcal{E})$. As stated in the Introduction, that part of the spectral function for ^{4}He has been taken to be $\mathcal{P}_1(p,\mathcal{E})=\mathcal{N}(p)\mathcal{P}_1^{\rm model}(p,\mathcal{E})$, where $\mathcal{P}_1^{\rm model}(p,\mathcal{E})$ has been provided to us by Ciofi degli Atti [6]. The normalization factor $\mathcal{N}(p)$ is fixed by

$$\int_{\mathcal{E}_{\rm thr}}^{\infty}d\mathcal{E}\mathcal{P}_1(p,\mathcal{E})=n(p)-n_0(p), \quad (2.12)$$

where the quantities $n(p)$, the total momentum distribution, and $n_0(p)$ have been calculated using the NR wave functions as will be explained in Sec. II B.

We have also tested the following simple two-state approximation for the spectral function [28,17]:

$$\mathcal{P}(p,\mathcal{E})\approx n_0(p)\,\delta(\mathcal{E})+[n(p)-n_0(p)]\,\delta(\mathcal{E}-\langle\Delta\rangle+\Delta_0),$$
$$\langle\Delta\rangle\approx 50\ \ \text{MeV}. \quad (2.13)$$

Substitution into Eq. (2.9) produces a $|\boldsymbol{q}|$-independent lowest order contribution,

$$\phi_0^{(1)}(y_G^{\Delta},y_G^{\Delta_0})=\frac{1}{4\pi^2}\left[\int_{|y_G^{\Delta}|}^{\infty}dp\,p\,n(p)-\int_{|y_G^{\Delta}|}^{|y_G^{\Delta_0}|}dp\,p\,n_0(p)\right]. \quad (2.14)$$

Since in the relevant p region $n_0\approx n$, an accurate approximation of Eq. (2.14) reads

$$\phi_0^{(2)}(y_G^{\Delta_0})\approx\frac{1}{4\pi^2}\int_{|y_G^{\Delta_0}|}^{\infty}dp\,p\,n(p). \quad (2.15)$$

Terms with $n\geqslant 1$ in Eq. (2.8) describe FSI corrections to the asymptotic limit as a series in $1/|\boldsymbol{q}|$. It is easier to give those in terms of their Fourier transform $\tilde{\phi}_n(s)$, namely

$$\phi_n(y_G^{\Delta})=\int_0^{\infty}\frac{ds}{2\pi}e^{isy_G^{\Delta}}\tilde{\phi}_n(s). \quad (2.16)$$

Each $\tilde{\phi}_n(s)\equiv\tilde{\phi}_n(s;[V])$ is a functional of the bare interaction V, for instance,

$$\frac{M}{|\boldsymbol{q}|}\tilde{\phi}_1(s)=\int d\boldsymbol{r}_1\int d\boldsymbol{r}_2\rho_2(\boldsymbol{r}_1,\boldsymbol{r}_2;\boldsymbol{r}_1-s\hat{\boldsymbol{q}},\boldsymbol{r}_2)[i\tilde{\chi}_q(\boldsymbol{b},z;s)], \quad (2.17a)$$

$$\tilde{\chi}_q(\boldsymbol{b},z;s)=\tilde{\chi}_q^{(1)}(\boldsymbol{b},z;s)+\tilde{\chi}_q^{(2)}(\boldsymbol{b},z;s), \quad (2.17b)$$

$$\tilde{\chi}_q^{(1)}(\boldsymbol{b},z;s)=-\frac{M}{|\boldsymbol{q}|}\int_0^s d\sigma V(\boldsymbol{b},z-\sigma), \quad (2.17c)$$

$$\tilde{\chi}_q^{(2)}(\boldsymbol{b},z;s)=\frac{M}{|\boldsymbol{q}|}sV(\boldsymbol{b},z-s)=-s\frac{\partial}{\partial s}\tilde{\chi}_q^{(1)}(\boldsymbol{b},z;s), \quad (2.17d)$$

where $\boldsymbol{b}$ (z) is the component of the vector $\boldsymbol{r}=\boldsymbol{r}_1-\boldsymbol{r}_2$ perpendicular (parallel) to the $\boldsymbol{q}$ direction, and ρ_2 is the semidiagonal two-particle density matrix. Equations (2.17) define two parts of the off-shell eikonal phase $\tilde{\chi}_q$ which are related, and thus

$$\tilde{\chi}_q(\boldsymbol{b},z;s)=\left(1-s\frac{\partial}{\partial s}\right)\tilde{\chi}_q^{(1)}(\boldsymbol{b},z,s). \quad (2.18)$$

One frequently deals with interactions V which have a strong short-range repulsion (or produce for other reasons a diffractive elastic amplitude) and it is then of advantage to perform a summation over a ladder of bare interactions V. The replacement $V\rightarrow V_{eff}=t_q$, produces a well-behaved, q-dependent, off-shell t matrix as an effective interaction, which in coordinate space is proportional to the off-shell profile function $\tilde{\Gamma}$ [10]. For the part $\tilde{\Gamma}^{(1)}$, generated by $\tilde{\chi}^{(1)}$, one has

$$i\tilde{\chi}_q^{(1)}(\boldsymbol{b},z;s)\rightarrow\tilde{\Gamma}_q^{(1)}(\boldsymbol{b},z;s)=\exp[i\tilde{\chi}_q^{(1)}(\boldsymbol{b},z;s)]-1 \quad (2.19a)$$

$$\approx\theta(z)\,\theta(s-z)\Gamma_q^{(1)}(b). \quad (2.19b)$$

The approximation Eq. (2.19b) has been tested in Ref. [29]. Its application permits the exploitation of a standard parametrization of the on-shell profile $\Gamma_q^{(1)}(b)$ in terms of elastic NN scattering data, as are $\sigma_q^{tot},\tau_q,Q_q^{(0)}$, which are, respectively, the total cross section, the ratio of the real to imaginary part of the forward elastic amplitude, and the width of the diffractive amplitude. Explicitly,

TABLE I. Selection of cross section ratios He/C, C/Fe. For given angle we give x, Q^2 and the ratios. Former are from Ref. [13], latter from Ref. [11].

$\theta=20^\circ$			$\theta=25^\circ$			$\theta=30^\circ$		
x	Q^2	He/C	x	Q^2	He/C	x	Q^2	He/C
2.69	1.44	0.64	2.10	2.07	0.64	1.37	2.51	0.66
1.40	1.34	0.70	1.23	1.88	0.69	1.08	2.35	1.17
0.70	1.18	0.88	1.37	2.51	0.96	0.81	2.12	1.03

$\theta=15^\circ$			$\theta=30^\circ$		
x	Q^2	C/Fe	x	Q^2	C/Fe
2.49	1.05	0.82	1.95	3.38	0.70
1.02	0.97	1.18	1.37	3.09	0.98
0.65	0.91	0.97	1.01	2.79	1.04
0.43	0.83	1.00	0.72	2.43	1.00

$$\Gamma_q^{(1)}(b)\approx\frac{1}{2}\sigma_q^{tot}(1-i\tau_q)\frac{[Q_q^{(0)}]^2}{4\pi}e^{-[bQ_q^{(0)}]^2/4}. \quad (2.20)$$

There is no simple way to generalize Eq. (2.18) to the total off-shell phase $\tilde{\chi}$. Yet, as in Ref. [10] we shall assume that Eq. (2.18) is also approximately valid for the total off-shell profile function

$$i\tilde{\chi}_q(\boldsymbol{b},z;s)\to\tilde{\Gamma}_q(\boldsymbol{b},z;s)\approx\left[1-s\frac{\partial}{\partial s}\right]\tilde{\Gamma}_q^{(1)}(\boldsymbol{b},z;s) \quad (2.21a)$$

$$\approx\left[1-s\frac{\partial}{\partial s}\right]\theta(z)\,\theta(s-z)\Gamma_q^{(1)}(b). \quad (2.21b)$$

After substitution of the above expression in Eq. (2.17), the leading FSI contribution to $\tilde{\phi}(\boldsymbol{q},s)$ turns into the following q-dependent result [10]:

$$\frac{M}{|\boldsymbol{q}|}\tilde{\phi}_1(s;[V])\to\frac{M}{|\boldsymbol{q}|}\tilde{\phi}_1(s,[t])=\tilde{G}_1(|\boldsymbol{q}|,s)$$
$$=\tilde{G}_1^{(1)}(|\boldsymbol{q}|,s)+\tilde{G}_1^{(2)}(|\boldsymbol{q}|,s), \quad (2.22)$$

where

$$\tilde{G}_1^{(1)}(|\boldsymbol{q}|,s)\approx-\int d\boldsymbol{r}_1\int d\boldsymbol{r}_2\rho_2(\boldsymbol{r}_1,\boldsymbol{r}_2;\boldsymbol{r}_1-s\hat{\boldsymbol{q}},\boldsymbol{r}_2)\,\theta(z)$$
$$\times\theta(s-z)\Gamma_q^{(1)}(b), \quad (2.23a)$$

$$\tilde{G}_1^{(2)}(|\boldsymbol{q}|,s)\approx\int d\boldsymbol{r}_1\int d\boldsymbol{r}_2\rho_2(\boldsymbol{r}_1,\boldsymbol{r}_2;\boldsymbol{r}_1-s\hat{\boldsymbol{q}},\boldsymbol{r}_2)s\,\theta(z)$$
$$\times\delta(s-z)\Gamma_q^{(1)}(b). \quad (2.23b)$$

Previous analyses dealt with targets with $A\geqslant 12$. For those there do not exist computations from first principles for single-nucleon momentum distributions $n_0(p)$, $n(p)$, and density matrices ρ_2, as required in Eqs. (2.11), (2.12), and (2.23). Moreover, suggested parametrizations [7,12] do not account for nucleon recoil, which is only justified for $A\gtrsim 12$.

One of the implications of Eq. (2.2) is a weak-A dependence of the SF for point-nucleon nuclei and of the averaged nucleon SF [10]. This entails predicted inclusive cross sections per nucleon to be practically independent of A. Supporting evidence comes from experimental ratios of cross sections per nucleon for different targets at identical kinematical conditions [10,11,30]. Definitely larger deviations from smooth A dependence are expected, if one of the targets is a light nucleus with $A\leqslant 6$. This is evident from Table I where we entered some C/Fe ratios from JLab data [31] and for He/C from the older NE3 data in Ref. [13].

For the above reasons, we did not include in the past a GRS analysis of inclusive scattering on the lightest targets. In the following we exploit the possibility to compute a precise NR nuclear ground state wave function Φ_0 of light nuclei for given nuclear interaction V. Those enable a calculation of $n(p), n_0(p)$ and ρ_2, which enter the components (2.11), (2.12), and (2.23) of the nuclear SF.

B. The density matrices

Various methods permit nowadays an accurate calculation of the ^{4}He ground state wave function [32]. We exploit here the correlated hyperspherical harmonic (CHH) function technique which has been developed by the Pisa group. The spatial configuration of the system is described in terms of a given choice of the Jacobi vectors $\boldsymbol{\xi}_1$, $\boldsymbol{\xi}_2$, $\boldsymbol{\xi}_3$. In the hyperspherical framework we use as new variables the hyperradius ρ, defined by

$$\rho^2=\sum_{i=1}^{3}\xi_i^2, \quad (2.24)$$

and the set $\Omega=\{\hat{\xi}_1,\hat{\xi}_2,\hat{\xi}_3,\varphi_2,\varphi_3\}$. The latter includes the polar angles $\hat{\xi}_i\equiv(\theta_i,\phi_i)$ of each Jacobi vector and additional hyperspherical angles φ_2, φ_3. We then write for the ground state wave function Φ_4,

TABLE II. Binding energies in MeV of ^{4}He calculated with the CHH method using the AV18 and AV18/UIX, and the older AV14 and AV14/UVIII, Hamiltonian models. Also listed are the corresponding ''exact'' GFMC results [37] as well as the experimental value.

Model	CHH	GFMC
AV18	24.0	24.1(1)
AV18/UIX	28.1	28.3(1)
AV14	24.0	24.2(2)
AV14/UVIII	27.5	28.3(2)
Expt.	28.3	

$$\Phi_4 = \sum_{n=1}^{N_{tot}} \left[\frac{u_n(\rho)}{\rho^4} \mathcal{A}\{\mathcal{F}_n(r_{12},r_{13},r_{14},r_{23},r_{24},r_{34})\mathcal{Y}_n(\Omega)\} \right], \tag{2.25}$$

where $\mathcal{A}$ is an antisymmetrizer and $\mathcal{Y}_n(\Omega)$ are the four-body hyperspherical harmonic (HH) functions [33]. Choosing $\mathcal{F}_n = 1$, Eq. (2.25) generates an uncorrelated HH expansion for the ^{4}He ground state wave function. For it, the rate of convergence is extremely slow when the *NN* interaction is strongly repulsive at small distances. One accounts for the latter property by multiplying every HH function in the expansion with a suitably chosen correlation factor $\mathcal{F}_n$, ultimately leading to the CHH expansion. The latter much improves the description of the target wave function for small internucleon distances, and a much smaller number of basis functions is required to get convergence.

In the case of ^{4}He, the correlation factors have been chosen to be of the Jastrow form [34]

$$\mathcal{F}_n = f_n(r_{12})g_n(r_{13})g_n(r_{14})g_n(r_{23})g_n(r_{24})g_n(r_{34}), \tag{2.26}$$

i.e., products of one-dimensional functions f_n and g_n which are solutions of a *NN* Schrödinger-like equation (for details, see Ref. [34]).

Using the Rayleigh-Ritz variational principle for varying functions u_n in Eq. (2.25),

$$\langle \delta_u \Phi_4 | H - E | \Phi_4 \rangle = 0, \tag{2.27}$$

one is led to a set of hyper-radial equations for the functions u_n in the variable ρ which, after discretization, is converted into a generalized eigenvalue problem and are solved by standard numerical techniques [35]. One thus determines the hyperradial functions $u_n(\rho)$ in Eq. (2.25) and the bound state energy E. We shall present below results based on (1) the Argonne V18 *NN* potential [36] (the AV18 model), (2) the Argonne V18 *NN* potential supplemented by the Urbana IX three-nucleon potential [37] (the AV18UR model), (3) the Argonne V14 *NN* potential [38] plus the Urbana VIII three-nucleon potential [39] (the AV14UR model).

The two models, which contain a three-nucleon interaction, provide a ^{4}He binding energy rather close to the experimental one, whereas the AV18 underbinds by about 4 MeV. The present status of the ^{4}He binding energy calculations with the CHH method is summarized in Table II, where in Eq. (2.25) up to $N_{tot} \approx 200$ functions have been used (the explicit CHH states included in the expansion are discussed in Ref. [34]).

Calculated binding energies for the AV18 or AV18UR Hamiltonians are within 1% of the ''exact'' Green's function Monte Carlo (GFMC) results [37] for corresponding interactions. Somewhat less satisfactory agreement between the CHH and GFMC results for the AV14UR model, since this interaction is more repulsive at short distances than the other two. For all we checked that our final results for the deep inelastic scattering cross sections depend only slightly on the value of N_{tot}, once $N_{tot} \gtrsim 200$.

The thus constructed ground state wave function, readily gives the corresponding four body density matrices, in particular, the one nondiagonal in $'1'$,

$$\rho_4(\boldsymbol{r}_1,\boldsymbol{r}_2,\boldsymbol{r}_3,\boldsymbol{r}_4;\boldsymbol{r}_1',\boldsymbol{r}_2,\boldsymbol{r}_3,\boldsymbol{r}_4) = \Phi_4(\boldsymbol{r}_1,\boldsymbol{r}_2,\boldsymbol{r}_3,\boldsymbol{r}_4)\Phi_4(\boldsymbol{r}_1',\boldsymbol{r}_2,\boldsymbol{r}_3,\boldsymbol{r}_4). \tag{2.28}$$

Successive integrations over the diagonal coordinates 3,4, and eventually over coordinate 2, then furnish ρ_2 and ρ_1 nondiagonal in $'1'$. The total momentum distribution is the Fourier transform of ρ_1.

The partial momentum distribution $n_0(p)$ is obtained from the overlap of Φ_4 and the (^{3}H, ^{3}He averaged) three-nucleon ground state wave function Φ_3, namely,

$$n_0(p) = |a(p)|^2,$$

$$a(p) = \langle \Phi_3(1,2,3)\chi_4\eta_4 | j_0(pR_{123,4})\Phi_4(1,2,3,4) \rangle, \tag{2.29}$$

where χ_4 (η_4) is the spin (isospin) state of particle 4, j_0 is the zero-order Bessel function, and $R_{123,4}$ is the distance of particle 4 with respect to the center of mass of the other three. The ground state wave function Φ_3 of the three-nucleon system has been obtained with the same Hamiltonian model used to generate Φ_4, and again by application of the CHH technique [35]. In Eq. (2.29), Φ_3 and $\chi_4\eta_4$ are coupled to give a state with vanishing total angular momentum and isospin.

Equations (2.23) for $\tilde{G}$ invite to express ρ_2 in terms of the variables $\boldsymbol{r} = \boldsymbol{r}_1 - \boldsymbol{r}_2$ and $\boldsymbol{R} = (\boldsymbol{r}_1 + \boldsymbol{r}_2)/2$ and then to perform the $\boldsymbol{R}$ integration

$$B(\boldsymbol{b},z;s) = \int d\boldsymbol{R}\rho_2(\boldsymbol{r}_1,\boldsymbol{r}_2;\boldsymbol{r}_1 - s\hat{\boldsymbol{q}},\boldsymbol{r}_2). \tag{2.30}$$

The result is substituted into Eqs. (2.23) and subsequently integrated over $\boldsymbol{b}$ and z.

C. An effective IS series

In Ref. [3], one may find a detailed account of the lowest order plane wave impluse approximation (PWIA) calculations as part of the IS series. To it one should perturbatively add FSI's due to the interaction of the knocked-out nucleon and the spectator core.

In the Introduction we recalled a recent proof [9,2] that the GRS and IS, both evaluated to order $O(1/|\boldsymbol{q}|^2)$, produce the same result. The lowest order is given by

$$\phi_0(|\boldsymbol{q}|,y_0)=\int_{|y_0|}^{2|\boldsymbol{q}|+y_0}\frac{dpp}{4\pi^2}\int_0^{\bar{E}_M}d\mathcal{E}\mathcal{P}(p,\mathcal{E})$$

$$+\theta(y_0)\int_0^{y_0}\frac{dp\,p}{4\pi^2}\int_{\bar{E}_m}^{\bar{E}_M}d\mathcal{E}\mathcal{P}(p,\mathcal{E}), \quad (2.31)$$

where in this case [3,9]

$$\bar{E}_m^M=\sqrt{M^2+(y_0+|\boldsymbol{q}|)^2}-\sqrt{M^2+(p\mp|\boldsymbol{q}|)^2}. \quad (2.32)$$

Above, y_0 is the IS scaling variable defined by [3,9]

$$y_0=y_0^\infty(1+\delta_0),$$

$$y_0^\infty=-|\boldsymbol{q}|+\sqrt{(\nu-\Delta_0)(\nu-\Delta_0+2M)},$$

$$\delta_0\approx-\frac{1}{2A'}\left[\frac{1+\nu/M}{1+|\boldsymbol{q}|/y_0^\infty}\right]+O(1/A'^2). \quad (2.33)$$

The IS first order is then obtained from the prescription that puts $\tilde{G}_1^{(2)}=0$ in Eq. (2.22) and simultaneously replaces the GRS scaling variable y_G^Δ, Eq. (2.7), by y_0 in Eq. (2.16). Finally, $f^{PN,A}(x,Q^2)$ is now calculated using again y_0 in place of y_G^Δ in Eq. (2.6). Those changes have been shown to generate the IS series to order $1/|\boldsymbol{q}|$ [2]. Actual applications will be given in the following section.

III. RESULTS

In this section, we present numerical results for inclusive cross sections on ^{4}He based on Eqs. (2.1) and (2.2). Unless stated differently, those results use density matrices based on the AV18UR interaction and the full spectral function as discussed in Sec. II A. In the GRS approach, the cross sections have been computed by approximating the reduced structure function as follows:

$$\phi(|\boldsymbol{q}|,y_G)\to\phi_0(|\boldsymbol{q}|,y_G^{\Delta_0}), \quad \text{0th order}, \quad (3.1)$$

$$\phi(|\boldsymbol{q}|,y_G)\to\phi_0(|\boldsymbol{q}|,y_G^{\Delta_0})+G_1(|\boldsymbol{q}|,y_G^{\Delta_0})\equiv\phi_{01}(|\boldsymbol{q}|,y_G^{\Delta_0}),$$

$$(0+1)\text{th order}, \quad (3.2)$$

where ϕ_0 is given by Eq. (2.9) and G_1 is the inverse Fourier transform of the functions given in Eq. (2.23). The corresponding IS expressions are obtained as discussed in Sec. II C.

In Fig. 1, we display the SLAC-Virginia NE3 cross section data [13] for $E=3.595$ GeV, scattering angles $\theta=16°$, 20°, 25°, 30° and varying energy loss ν, and also our numerical results obtained with the above reduced response ϕ_{01}. Table III shows the ranges of the kinematical variables x,ν,Q^2. For all measured scattering angles, and in addition for $\theta=45°$, we entered there values of the energy loss ν and

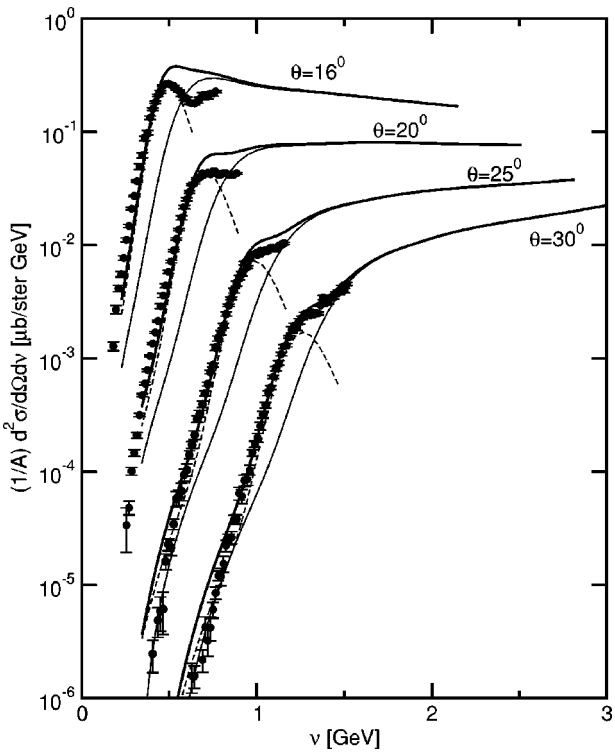

FIG. 1. Predicted cross sections for inclusive scattering of 3.595 GeV electrons from ^{4}He as function of the energy loss ν and for four values of the scattering angles θ in the $(0+1)$th order approximation (thick solid lines). Thin dashed (solid) lines show the NE (NI) part of the cross sections. Data are from Ref. [13].

of Q^2 close to the appropriate lower ($x=2$) and upper ($x=0.1$) ends of the theoretical curves shown in Fig. 1. We also show the ν,Q^2 values corresponding to the position of the QEP at $x=1$.

Let us first focus on the NE part of the cross section (thin dashed lines), which contributes primarily around the QEP. As can be seen from the figure, the NE parts well describe the QEP, in particular at low Q^2. The data for $\theta=16°$ show a clear maximum and an adjacent minimum which get fuzzier and ultimately disappear for increasing θ or Q^2. The same maximum occurs in the inclusive cross sections on deuterons [40], but is absent for targets with $A\geqslant 12$ [13,31].

TABLE III. Values of ν (in GeV) and Q^2 (in GeV^2) for $E=3.6$ GeV [13]. The selected values of x correspond approximately to the QEP and the lower and upper ends of the curves shown in Fig. 1.

	Lower end $x=2$		QEP $x=1$		Upper end $x=0.1$	
θ	ν	Q^2	ν	Q^2	ν	Q^2
16°	0.25	0.93	0.46	0.87	2.00	0.44
20°	0.37	1.40	0.68	1.27	2.50	0.48
25°	0.55	2.06	0.95	1.79	2.80	0.54
30°	0.74	2.76	1.22	2.29	3.00	0.58
45°	1.23	4.99	1.90	3.58	3.31	0.62

This structure is the result of the competition between the NE and the NI parts of the cross section. For decreasing Q^2 the NE part around the QEP $x=1$ grows relative to the, usually dominant, NI part. For the smallest Q^2 in the data, the NE part beyond the QEP stands out until for $x \lesssim 1$ the NI one overtakes. It is the maximum value of $f^{PN,A}(x,Q^2)$ (for $x \approx 1$) which sets the magnitude of the QEP. For a given Q^2, that peak value decreases with A: it is largest for the deuteron and ^{4}He and then it is almost independent on A for $A \geqslant 12$, reflecting the smearing of the momentum distribution due to the Fermi motion. For example, $f^{PN,A}(x=1,Q^2)$ for the deuteron and ^{4}He is ≈ 5.5 and 2.2 times, respectively, larger than for nuclei with $A \geqslant 12$. It causes the QEP for equal kinematic conditions to be most prominent for the lightest nuclei.

We already mentioned that Eq. (2.2) (for the NI part) is estimated to be valid for $x \gtrsim 0.2$ and above some critical $Q_c^2 \approx 2.0$–2.5 GeV^2 [10,11]. As Table III shows, that approximate critical value is actually never reached for any $\theta = 16°, 20°$ data point, which renders those data not really suitable for a test of the theory. For the same reason we excluded from our analysis NE3 data at lower energies and the same is the case for old, near-elastic, high-Q^2 data on ^{4}He [41]. For both angles, the convolution formula predicts too large NI parts around the QEP, resulting in an overprediction of the data in that region. For $\theta = 30°$, on the other hand, $Q^2 \gtrsim Q_c^2$ and, in fact, comparison of data and computed results shows that there is good agreement for all but the smallest energy loss values. Since cross sections there have fallen by orders of magnitude, one expects sensitivity to small dynamical details. For example, without the inclusion in Eq. (2.2) of the mixing factor C_{22}, Eq. (2.4), the agreement would be of definitely lower quality (see also below).

With respect to the misfit for low angles around $x=1$, the use of nucleon SF's averaged over resonances may be the cause [42]. In fact, nucleon resonances influence the immediate region around $x=1$, and this effect is expected to decrease with increasing Q^2.

A more stringent test for the theory would be provided by data at higher beam energies with, in general, higher Q^2. Unfortunately, the recent 4-GeV experiments at JLab for various targets did not contain ^{4}He [31], but a recent JLab proposal includes that target in a 6-GeV run with scattering angles $\theta = 15°$, 23°, 30°, 45°, and 60° [18]. The kinematical region explored by that experiment covers $0.2 < x < 1.0$ and $1 < Q^2 < 8.0$ GeV^2 (Table IV) and predictions for the four largest scattering angles can be found in Fig. 2. Incidentally, we checked that for $E=6$ GeV the effect of C_{22} is practically negligible due to Q^2, which grows with beam energy E.

Next we discuss the effect of the different approximations for ϕ_0 presented in Sec. II. The cross sections calculated using the approximations (2.14) and (2.15) for ϕ_0 almost overlap. Moreover, they are rather similar to the ones computed using the spectral function, Eq. (2.9), except in the low-ν region. There, the use of the ''full'' model slightly reduces the cross sections.

This result deserves some comment. The differences between the two expressions, Eqs. (2.9) and (2.15) are generally sizable in particular in the low-ν region [3] where $y_G^{\Delta_0}$ is negative and large in absolute value. However, in the kinematical region of the NE3 experiment, the values of E_M entering Eq. (2.9) are found to be rather large and then

$$\int_0^{E_M} d\mathcal{E}\mathcal{P}(p,\mathcal{E}) \approx \int_0^{\infty} d\mathcal{E}\mathcal{P}(p,\mathcal{E}) = n(p). \tag{3.3}$$

As a result, the ϕ_0 calculated using Eq. (2.9) or (2.15) nearly coincide. For example, for $E=3.595$ GeV, $\theta=30°$, and $\nu = 0.7$ GeV, $|\boldsymbol{q}|/\nu \approx 3$ and E_M is large for all the values of p. For the same reason we expect that the predicted cross sections do not much depend on the parametrization chosen for the spectral function, in particular, not in the low-ν region. In that region they are rather sensitive to the tail of the momen-

TABLE IV. Values of ν (in GeV) and Q^2 (in GeV^2) for $E = 6.0$ GeV and the values of θ of the proposed Jefferson Lab experiment. The selected values of x correspond approximately to the QEP and the lower and upper ends of the curves shown in Fig. 2.

	Lower end $x=2$		QEP $x=1$		Upper end $x=0.1$	
θ	ν	Q^2	ν	Q^2	ν	Q^2
23°	1.21	4.56	2.02	3.80	5.01	0.94
30°	1.80	6.75	2.77	5.20	5.37	1.01
45°	2.90	10.90	3.91	7.34	5.70	1.07
60°	3.69	13.86	4.57	8.58	5.82	1.09

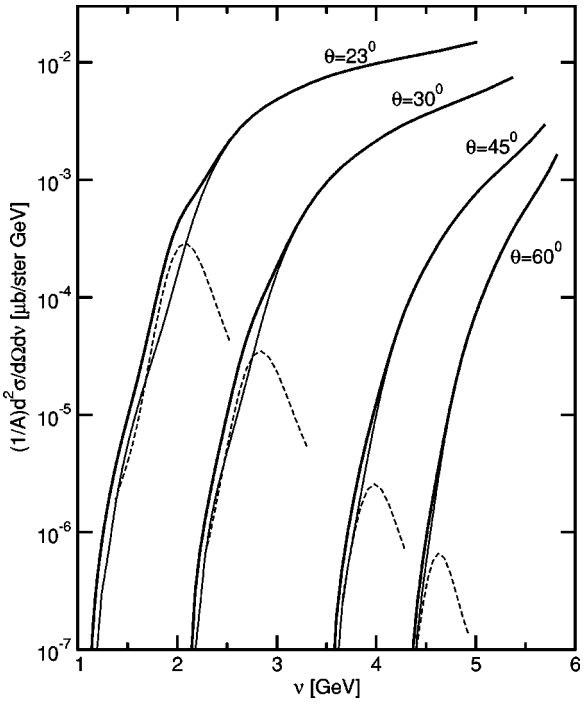

FIG. 2. Predicted cross sections for inclusive scattering of 6.0 GeV electrons from ^{4}He as function of the energy loss ν and for four values of the scattering angles θ in the $(0+1)$th-order approximation (thick solid lines). Thin dashed (solid) lines show the NE (NI) part of the cross sections.

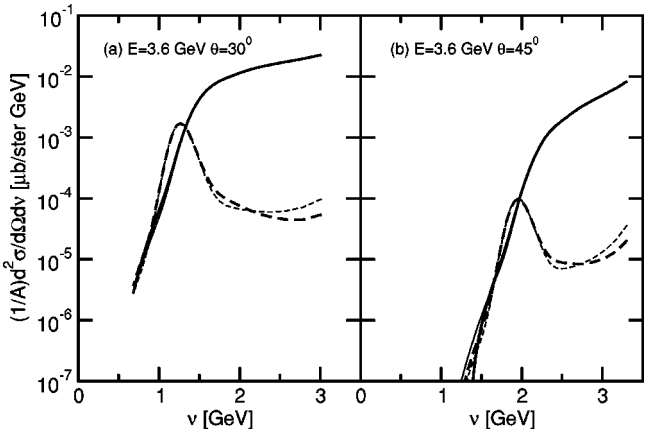

FIG. 3. (a) Contributions to the cross section for $E=3.595$ GeV, $\theta=30°$ from the NE (dashes) and the NI (solid lines) parts of the nucleon SF. Thin and thick lines are computed from the 0th- and $(0+1)$th-order reduced response $\phi(|\boldsymbol{q}|,y_G)$, respectively. The density matrices correspond to the AV18UR nuclear interaction. (b) The same as in (a), but for $\theta=45°$.

tum distributions, which in turn is related to the correlations in the nuclear wave functions [43].

In Fig. 3(a), we display the separate contributions of the cross sections at $E=3.595$ GeV, $\theta=30°$, and varying ν, as due to the NE and NI components of the nucleon SF $F_k^{\langle N\rangle}$. The thin (heavy) dashes are NE parts in the ϕ_0 (ϕ_{01}) approximation for the reduced response. Those have their maximum at $x\approx 1$, and are only in the wings marginally affected by the first-order FSI terms. The thin and heavy solid lines show the corresponding NI parts, which by nature dominate the region $x\lesssim 1$ for relatively high ν. FSI affect only the low-ν region and cause a rather small increase in cross sections. In those ν regions, NE and NI parts are of the same order. Figure 3(b) is as Fig. 3(a) for $\theta=45°$ (this angle was chosen since the Q^2 values are larger and similar to those for $E=6$ GeV, $\theta=15°$). The results are similar, except that FSI's now appear to decrease the zeroth NI contribution at low ν.

From Fig. 3(a) we observe that the slight overprediction in the low-ν region of the theoretical results at $\theta=30°$ is mainly due to the NI part and as discussed above, is only marginally affected by the inclusion of FSI. The reason for the large NI contribution can be simply understood by looking at the convolution (2.2) between the nucleon SF and $f^{PN,A}$.

Typical behavior of the functions $f^{PN,A}(z,Q^2)$, $F_2^{\langle N\rangle,\mathrm{NI}}(x/z,Q^2)$ and the mixing factor $C_{22}(Q^2/x^2,z)$, (the latter two for $x=0.1$, 2.0) are given in Fig. 4 ($F_1^{\langle N\rangle,\mathrm{NI}}$ behaves similarly). For $x<1$, the permitted range of values $z\geqslant x$ covers the $z\approx 1$ region where $f^{PN,A}(z,Q^2)$ is large and allows virtually the entire support x/z of $F^{\langle N\rangle,NI}$ to contribute. In contrast, for $x>1$ [see Fig. 4(b)], only the tail of $f^{PN,A}$ contributes and $F^{\langle N\rangle,\mathrm{NI}}(t,Q^2)$ for $x/A\leqslant t\leqslant 1$ is usually small. Moreover, $f^{PN,A}$ decreases as $z\to 4$. In fact, as z becomes larger, also $|y_G^{\Delta_0}|$ increases and the integral in Eq. (2.9) decreases. However, $y_G^{\Delta_0}\approx -\sqrt{Q^2}/2$ for $z\gg 1$ and since the values of Q^2 in the $E=3.595$ GeV NE3 experiment are

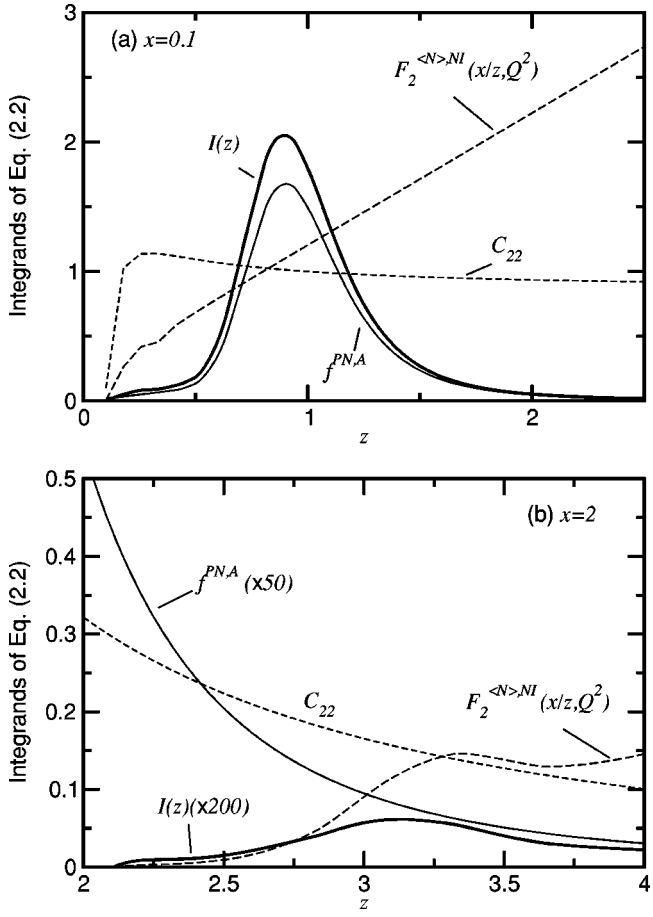

FIG. 4. The GRS function $f^{PN,A}(z,Q^2)$ (thin solid line), the nucleon SF $F_2^{\langle N\rangle,\mathrm{NI}}(x/z,Q^2)$ (long dashed line) and the mixing factor $C_{22}(Q^2/x^2,z)$ (short dashed line) entering Eq. (2.2) as function of z for $E=3.595$ GeV, $\theta=30°$ and two cases of x: (a) $x=0.1$ (corresponding to have $Q^2=0.58$ GeV^2, $\nu=3.00$ GeV) and (b) $x=2$ ($Q^2=2.76$ GeV^2, $\nu=0.74$ GeV). $I(z)$ is the corresponding integrand of Eq. (2.2). All functions above are dimensionless.

not large, ϕ_0 and the corresponding $f^{PN,A}$ are still nonvanishing at $z\to 4$. As a consequence, the integrals receive a sizable contribution from the region $z>3$ and the NI cross section in the low ν region remains large.

Note also that the mixing factor $C_{22}\approx 1$ for $x=0.1$ [Fig. 4(a)] but is rather small for $x=2$ [Fig. 4(b)], sizably reducing the NI part of the cross section in that region. As stated before, without the inclusion of such a factor C_{22}, the overprediction of the theoretical cross section in the low-ν-region would be more pronounced.

Next, applying the prescription recalled in Sec. II C, we make a comparison between GRS and IS cross sections for $E=3.595$ GeV. Figure 5(a) (5b) shows the results for $\theta=30°$ using the ϕ_0 (ϕ_{01}) approximation for the reduced response, together with the NE3 data. The agreement between the two calculated results is good, but not perfect. One of the causes is undoubtedly the use of Eq. (2.21), which is an approximation for the parametrized, off-shell total profile function $\tilde{\Gamma}$, and of course not intrinsic to the actual ladder summation. Also the agreement with the data is good, except for the smallest ν.

One observes that the GRS and IS results using only ϕ_0

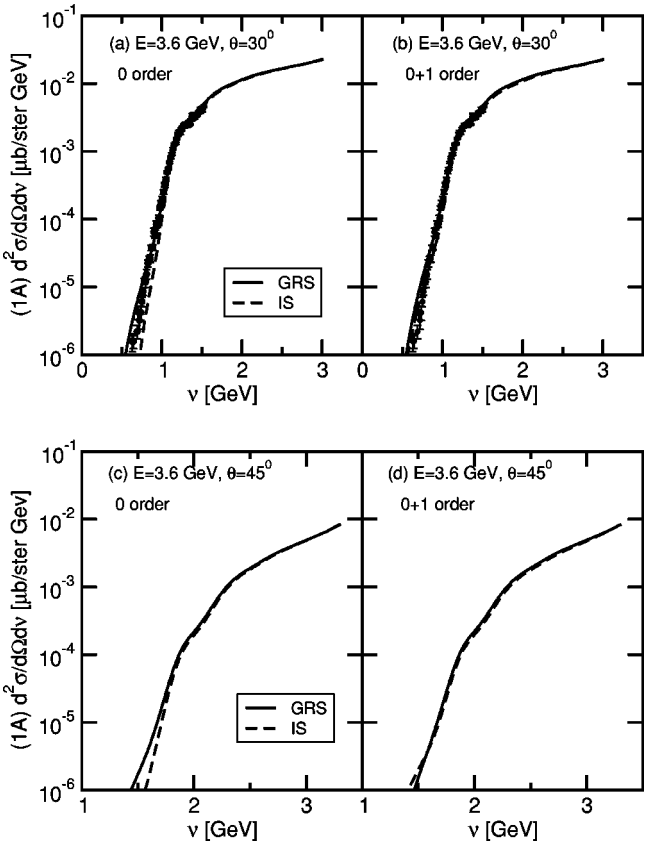

FIG. 5. (a) Comparison of the zeroth order GRS and derived IS cross sections for $E=3.595$ GeV, $\theta=30°$. (b) As in (a) but in the case of the $(0+1)$th order. (c) and (d): as in (a) and (b), respectively, but for $\theta=45°$.

diverge for decreasing ν and that the GRS comes closest to the data. This is shown in Fig. 5(a) for $\theta=30°$, $E=3.595$ GeV, but holds in fact for all examined cases. Comparison of Figs. 5(a) and 5(b), moreover, shows that FSI's for GRS are smaller than for the IS, in particular for smaller ν. The two observations above can be understood theoretically [9] and have previously been demonstrated for simple models.

Finally, one infers from Fig. 5(b) that the differences between the zero-order IS and GRS cross sections are noticeably reduced when the first-order FSI is included in both calculations. A similar comparison is shown in Figs. 5(c) and 5(d) for $\theta=45°$ and, again, the agreement is found to be good after the inclusion of the FSI.

The separate IS NE and NI parts for $E=3.595$ GeV and $\theta=30°$ ($\theta=45°$) are shown in Fig. 6(a) [Fig. 6(b)], where we used the same notation adopted in Fig. 3. In this case, the NI part computed with the ϕ_0 approximation for the reduced response (thin solid line) stays well below the NE one (thin dashed line) in the low ν region, as already found in Ref. [3]. Now, in the evaluation of the convolution (2.2), $|y_0|$ becomes rather large as $z\to 4$ and ϕ_0 rapidly decreases ($y_0\to -\sqrt{Q^2}$ as $z\gg 1$). As a consequence, the IS integrand of Eq. (2.2) is very small in the low-ν region (in contrast to what happens in the GRS case). Since much of the input is the same as used in Ref. [28], our lowest order results agree well with

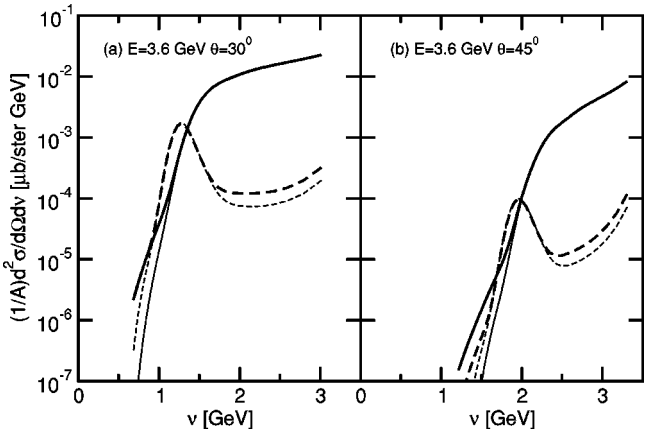

FIG. 6. As in Fig. 3 but for the IS case. (a) Contributions to the cross section for $E=3.595$ GeV, $\theta=30°$ from the NE (dashes) and the NI (solid lines) parts of the nucleon SF. Thin and thick lines are computed from the the 0th- and $(0+1)$th-order reduced response $\phi(|\boldsymbol{q}|,y_0)$, respectively. The density matrices correspond to the AV18UR nuclear interaction. (b) The same as in (a), but for $\theta=45°$.

those reported in that paper. However, as already discussed in relation with Fig. 5, the FSI's contributions in the IS case are sizable. In fact, those FSI's are given by Eq. (2.22) without the term $\tilde{G}_1^{(2)}$, which otherwise would partially cancel the contribution of the large term $\tilde{G}_1^{(1)}$. As a result, in the low-ν region, the IS NI cross section calculated at the level of the $(0+1)$th order becomes larger than the NE one, and rather close to the GRS NI cross section.

Another interesting aspect is the influence of the nuclear interaction, chosen to calculate the density matrices. In Fig. 7, we display for $E=3.595$ GeV, $\theta=30°$ cross sections computed on the basis of the three previously mentioned models of nuclear interaction (AV18UR, AV18, and AV14UR). The calculations have been performed using ϕ_0 from Eq. (2.15) with the density matrices determined directly from the corresponding nuclear wave functions. For identical kinematics the results for AV18UR and AV14UR can hardly

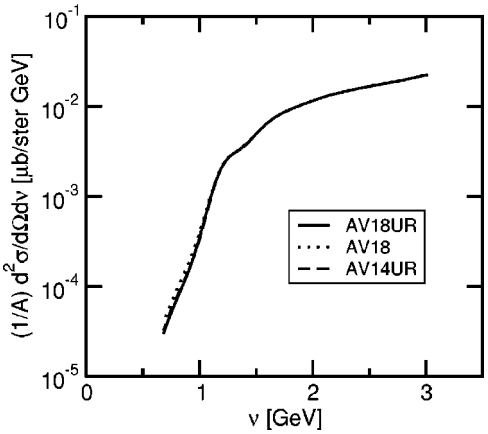

FIG. 7. $(0+1)$th-order GRS cross sections at $E=3.595$ GeV and $\theta=30°$ for the AV18 (dashed), AV14UR (long dashed), and AV18UR (solid) nuclear interactions.

be distinguished, whereas the AV18 cross section is slightly different from the other two in the low-ν tail: There clearly is only weak dependence on the nuclear interaction.

IV. CONCLUSIONS

We have studied inclusive scattering of high-energy electrons from ^{4}He, for energy losses below and around the quasielastic peak and up into the deep inelastic scattering region. The underlying model assumes noninterference between nucleonic and subnucleonic degrees of freedom, which implies that total nuclear structures function may be expressed as a generalized convolution of the structure functions of free nucleons and the one of a nucleus composed of point particles. The model is estimated to become gradually imprecise for $Q^2 \lesssim 2-2.5$ GeV^2. Structure functions for a nucleus of point particles are computed via the reduced response $\phi(q,y)$ using a relativistic generalization of the GRS series, which includes the first-order FSI.

A new element in the development of the latter is an actual calculation of the required single- and two-particle, semidiagonal density matrices, based on accurately computed ^{4}He ground state wave function. The above replaces previously used parametrizations of derived density matrices for targets with $A \geqslant 12$. Computed cross sections appear to be hardly dependent on the choice of the *NN* interaction.

In conclusion, we have found, first of all, that inclusive cross sections of electron on ^{4}He computed with the leading two terms in the GRS series are in good agreement with the NE3 SLAC-Virginia data for all scattering angles. The latter in spite of the fact that for $\theta \lesssim 30°$ the involved Q^2 fall below the validity estimate. Second, for all kinematical regions under study, the FSI's for GRS are smaller than for the IS, in particular for low-energy losses. Third, we have presented the first comparison between the GRS and IS expansions for a real nucleus, cut at the same order in $1/|\boldsymbol{q}|$. We have observed that they produce similar cross sections, in particular, after the inclusion of the corresponding FSI contributions.

We also presented predictions for a future $E=6$ GeV experiment at JLab on ^{4}He. Its kinematics are largely within the estimated limits of the underlying GRS theory and a comparison of computed results with data will be more significant for those than is the case for the NE3 data.

ACKNOWLEDGMENTS

The authors are grateful for having received from C. Ciofi degli Atti tables of numerical values of the ^{4}He spectral function, mentioned in Sec. II. One of us (M.V.) also gratefully acknowledges a helpful discussion with G. I. Lykasov.

[1] N.N. Nikolaev, J. Speth, and B.G. Zakaharov, J. Exp. Theor. Phys. **82**, 1046 (1996); A. Bianconi, S. Jeshonnek, N.N. Nikolaev, and B.G. Zakaharov, Phys. Lett. B **343**, 13 (1995).
[2] A.S. Rinat and B.K. Jennings, Phys. Rev. C **59**, 3371 (1999).
[3] See, for instance, C. Ciofi degli Atti, E. Pace, and G. Salmè, Phys. Rev. C **43**, 1155 (1991); C. Ciofi degli Atti, D.B. Day, and S. Liuti, Phys. Lett. B **225**, 215 (1989); Phys. Rev. C **46**, 1045 (1992).
[4] O. Benhar, A. Fabrocini, S. Fantoni, G.A. Miller, V.R. Pandharipande, and I. Sick, Phys. Rev. C **44**, 2328 (1991); Phys. Lett. B **359**, 8 (1995).
[5] P. Fernandez de Cordoba, E. Marco, H. Mutter, E. Oset, and A. Faessler, Nucl. Phys. **A611**, 514 (1996).
[6] C. Ciofi degli Atti and S. Simula, Phys. Lett. B **325**, 276 (1994).
[7] H. Gersch, L.J. Rodriguez, and Phil N. Smith, Phys. Rev. A **5**, 1547 (1973).
[8] S.A. Gurvitz, Phys. Rev. C **42**, 2653 (1990).
[9] S.A. Gurvitz and A.S. Rinat, Phys. Rev. C **65**, 024310 (2002).
[10] A.S. Rinat and M.F. Taragin, Nucl. Phys. **A598**, 349 (1996); **A620**, 412 (1997); **A623**, 773(E) (1997).
[11] A.S. Rinat and M.F. Taragin, Phys. Rev. C **60**, 044601 (1999).
[12] A.S. Rinat, Phys. Rev. B **40**, 6625 (1989); A.S. Rinat, M.F. Taragin, F. Mazzanti, and A. Polls, *ibid.* **57**, 5347 (1998).
[13] D.B. Day *et al.*, Phys. Rev. C **48**, 1849 (1993).
[14] H. Morita and T. Suzuki, Prog. Theor. Phys. **86**, 671 (1991).
[15] V.D. Efros, W. Leidemann, and G. Orlandini, Phys. Rev. C **58**, 582 (1998).
[16] C. Ciofi degli Atti and G.B. West, Phys. Lett. B **458**, 447 (1999).
[17] V.D. Efros, W. Leidemann, and G. Orlandini, Phys. Lett. B **338**, 130 (1994); Phys. Rev. Lett. **78**, 432 (1997).
[18] J. Arrington (spokesperson), Jefferson Lab Proposal Report No. E-00-101, 2000.
[19] N. Poliatzki and S.A. Gurvitz, Nucl. Phys. **A524**, 217 (1991).
[20] S.A. Gurvitz and A.S. Rinat, Report No. TR-PR-93-77/ WIS-93/97/Oct-PH; Prog. Part. Nucl. Phys. **34**, 245 (1995).
[21] A.S. Rinat, in *Proceedings of the Second International Conference on Perspectives in Hadronic Physics, ICTP, Trieste, Italy, 1999*, edited by S. Boffi *et al.* (World Scientific, Singapore, 1999), p. 62.
[22] A.S. Rinat and M.F. Taragin, Phys. Rev. C **62**, 034602 (2000).
[23] G.B. West, Ann. Phys. (N.Y.) **74**, 646 (1972); W.B. Atwood and G.B. West, Phys. Rev. D **7**, 773 (1973).
[24] C.H. Llewellyn Smith, Phys. Lett. **128B**, 117 (1983); M. Ericson and A.W. Thomas, *ibid.* **128B**, 120 (1983).
[25] A. Bodek and J.L. Ritchie, Phys. Rev. D **23**, 1070 (1981).
[26] P. Amadrauz *et al.*, Phys. Lett. B **295**, 159 (1992); M. Arneodo *et al.*, *ibid.* **364**, 107 (1995).
[27] A. S. Rinat and M. F. Taragin, Phys. Lett. B **551**, 284 (2003).
[28] C. Ciofi degli Atti and S. Simula, Phys. Rev. C **53**, 1689 (1996).
[29] A.S. Rinat and M.F. Taragin, Nucl. Phys. **A623**, 519 (1997).
[30] J. Arrington *et al.*, Phys. Rev. C **53**, 2248 (1996).
[31] J. Arrington *et al.*, Phys. Rev. Lett. **82**, 2056 (1999).
[32] H. Kamada *et al.*, Phys. Rev. C **64**, 044001 (2001).
[33] M. Fabre de la Ripelle, Ann. Phys. (N.Y.) **147**, 281 (1983).
[34] M. Viviani, A. Kievsky, and S. Rosati, Few-Body Syst. **18**, 25 (1995).

[35] A. Kievsky, S. Rosati, and M. Viviani, Nucl. Phys. **A577**, 511 (1994).
[36] R.B. Wiringa, V.G.J. Stoks, and R. Schiavilla, Phys. Rev. C **51**, 38 (1995).
[37] B.S. Pudliner *et al.*, Phys. Rev. C **56**, 1720 (1997).
[38] R.B. Wiringa, R.A. Smith, and T.L. Ainsworth, Phys. Rev. C **29**, 1207 (1984).
[39] R.B. Wiringa, Phys. Rev. C **43**, 1585 (1991).
[40] J. Arrington (private communication); I. Niculescu *et al.*, Phys. Rev. Lett. **85**, 1182 (2000).
[41] S. Rock *et al.*, Phys. Rev. **26**, 1592 (1982)
[42] J-P. Chen (private communication).
[43] See, for instance, O. Benhar, S. Fantoni, and G.I. Lykasov, Eur. Phys. J. A **5**, 137 (1999), and references therein.